Aerodynamic analysis of the wing flexibility and the clap-and-peel motion of the hovering DelFly II

T. Gillebaart*, A.H. van Zuijlen, and H. Bijl
Delft University of Technology, 2629 HS Delft, The Netherlands

ABSTRACT

A Micro Aerial Vehicle developed at the Delft University of Technology (DelFly II) uses flapping wings to produce the forces needed for forward flight and hovering. The DelFly II is inspired by the dragonfly with two flexible wings making a 'clap-and-peel' motion at each side of the body. In this paper the influence of wing flexibility and the 'clap-and-peel' motion (one versus two wings) on the upward (lifting) force in hover is studied. CFD simulations based on the ALE Navier-Stokes equations together with radial basis function mesh interpolation are used. For the 'clap-and-peel' motion an immersed symmetry plane is introduced into the computational domain. The flexible shapes of the wing are obtained from experiments. Preliminary results are shown for a flexible and an equivalent rigid wing. These results show that the use of a flexible wing increases the upward force for both the single wing motion and the 'clap-and-peel' motion. The 'clap-and-peel' motion increases the upward force per wing for both the flexible and rigid wing when compared to the single wing making the same motion. From the preliminary results it can be concluded that flexibility enhances the production of the upward force.

1 INTRODUCTION

Aerodynamic characteristics of flapping flight have been extensively studied during the past years (e.g. [1]). First only the main physical phenomena were investigated, such as the importance of the leading edge vortex [2]. More recently also the influence of flexible deforming wings has been the subject of these studies [3], for which CFD simulations have been increasingly used as an analytical tool. In [4, 5] a more fundamental study on flexibility showed the potential benefits of flexible wings over rigid wings. In these studies it is concluded that wing flexibility can be tailored such that the forces produced are higher than with a rigidly moving wing.
In 2005 a flapping MAV was developed at the TU Delft, named the DelFly [6], which has been used to study flapping flight. In [7] a first analysis of the aerodynamics of the hovering DelFly II has been made by use of PIV experiments. After this a study on the aerodynamics of different wing designs using again PIV experiments has been performed [8]. At the same time [9] studied several aspects of flapping wings using CFD simulations with moving meshes.
In this study the influence of wing flexibility and the 'clap-and-peel' motion on the upward (lifting) force in hover conditions is investigated using two-dimensional CFD simulations. To determine the influence of wing flexibility a wing with imposed flexibility and an equivalent rigid wing are simulated. Chord wise wing deformation of the DelFly II wing has been measured at several span wise locations [8]. These deformed wing shapes are used in this study to simulate the flexibility of the wing. In this study the novel approach is taken by enforcing the wing shapes instead of using full fluid-structure interaction. The interaction from the fluid to the structure is absent, which eliminates the necessity of a structural model of a complex 3D wing translated to 2D. However due to this there is no damping in the acceleration imposed from the wing on the fluid.
Earlier studies showed that the 'clap-and-peel' motion greatly enhances the upward force in flapping flight [10, 11]. In this study the influence of the 'clap-and-peel' motion on the upward force produced is investigated by comparing results for a single wing and a wing close to a mirror plane to model the presence of a second wing. The Reynolds number is relevant for MAV's (around 7000) and the imposed flexibility is based on a real wing of the DelFly II. For the 'clap-and-peel' motion a newly developed method is used based on a immersed symmetry plane together with mesh topology adjustments.

2 METHODS

The method to simulate the flapping wing is by solving the Arbitrary Lagrangian-Eulerian form of the unsteady, incompressible, laminar Navier-Stokes equations in OpenFOAM, which uses finite volume discretisation [12]. For the mesh movement radial basis function (RBF) mesh interpolation is used [13]. An immersed boundary method is used to impose symmetry plane conditions in the flow in case of 'clap-and-peel' motion.

2.1 2D incompressible flow simulations

Fluid flows are described by the Navier-Stokes equations. In case of small flapping wings, the Reynolds and Mach number may be small enough that the unsteady, incompressible, laminar Navier-Stokes equations can be used [9, 14, 15]. For

*Email address(es): t.gillebaart@student.tudelft.nl

now, only two-dimensional simulations are performed.
Since hovering is considered close attention should be given to the boundary conditions, because vortices shed by the wing are not convected downstream but can also leave the domain through the sides. Because of the zero velocity as far field condition, in and out flow can occur at the same place at different times. To achieve this the pressure and the velocity are coupled at the boundary by using a total pressure boundary condition. The total pressure at the boundary is set to a constant value and depending on the flow velocity the static pressure is set. The direction of the flow at the boundary is set based on the pressure difference at the boundary. When the pressure difference at the boundary indicates an outward flux this is coupled to the velocity by imposing an outward flow and vice versa. In this way the pressure and velocity can vary at the boundary in time and also cope with vortices leaving the domain. Other settings for OpenFOAM can be found in Table 1.

Setting	Values
p solver	Algebraic multi-grid
p tolerance	$1e^{-7}$
U solver	BiCGStab
U tolerance	$1e^{-9}$
PISO loops	2
Non-orthog. cor.	1 (only for double wing)
Courant nr.	0.4
$\frac{\partial}{\partial t}$	Backward differencing formula (2^{nd})
∇	Gaussian (2^{nd})
$\nabla\bullet$	Gaussian Gamma differencing (2^{nd})
∇^2	Gaussian linear corrected (2^{nd})
Mesh	59906 cells
Coarse mesh	15314 cells

Table 1: Settings for OpenFOAM.

To simulate the moving and deforming wing the mesh should deform accordingly. To accomplish this the Arbitrary Lagrangian-Eulerian (ALE) Navier-Stokes equations are used.

2.2 ALE Navier-Stokes with OpenFOAM

Simulating the fluid flow around flapping wings is done by using the Arbitrary Lagrangian-Eulerian Navier-Stokes equations [16]. The Eulerian description is still used for the fluid, but the moving mesh is described using the Lagrangian method. In Equation (1) the momentum equation of the unsteady, incompressible, laminar ALE Navier-Stokes is shown.

$$\begin{aligned} \frac{\partial}{\partial t}\int_{V_C}\mathbf{u}dV &+ \oint_{S_C}\mathbf{n}\cdot(\mathbf{u}-\mathbf{u}_{mesh})\mathbf{u}dS \\ &- \int_{V_C}\nabla\cdot(\nu\nabla\mathbf{u})dV \\ &= \int_{V_C}\frac{\nabla p}{\rho}dV \end{aligned} \quad (1)$$

Two terms in these equations are different from the standard momentum equation. Firstly the temporal term, which is different because the derivative cannot be placed inside the integral as the volume does change over time. Secondly in the convective term the mesh velocity can be found. Due to the movement of the faces an extra flux is created through the faces. Both these terms are caused by the movement of the mesh through the fluid and the deformation of the mesh cells. A (detailed) description on how this is used to simulate moving body aerodynamics can be found in [9]. For a more (detailed) description on the implementation in OpenFOAM, please see [17]. The reason for using this method is clearly explained in [18], which shows that as long as remeshing is not needed the ALE Navier-Stokes should be used to simulate moving and deforming body aerodynamics. Since only the movement of the wing is known the movement of the rest of the mesh should be interpolated based on the wing movement. This is done with radial basis function (RBF) mesh interpolation [13].

2.3 RBF mesh interpolation

Besides the equations to model the fluid, also an algorithm is needed to deform the mesh based on the wing movement. In [13] it is shown that RBF mesh interpolation is a promising mesh movement algorithm when considering the mesh quality and the simplicity of the implementation. Especially in rotation the RBF mesh interpolation performs better than alternative methods available in OpenFOAM [9]. In the flapping wing kinematics typically large rotations are present and therefore the RBF mesh interpolation is chosen as method for deforming the mesh based on the movement of the wing. RBF mesh interpolation is based on smooth interpolation from known displacements of the control points to the rest of the field using radial basis functions. In this study the control points are chosen such that the simulated wing is deformed as the wing shapes from the experiments. For the basis function evaluations only the euclidean distance between each control point and each internal point is needed. So no grid connectivity is needed, which makes this method easy to implement. RBF mesh interpolation provides a robust and easy method to deform the mesh smoothly when only the movement of the body is known. For more details on this method see [13].

2.4 Mesh quality in time

During the complete flapping period the mesh should preserve its quality to ensure reliable computations. By means of skewness and non-orthogonality the mesh quality is measured during a full period to determine which control points should be used. Since the DelFly II wing, which is made of a thin flexible foil, has a very small thickness a 'zero-thickness' wing is used in the simulations. In CFD simulations using OpenFOAM a 'zero-thickness' wing can be modelled by creating two rows of faces connected to the same points, but with

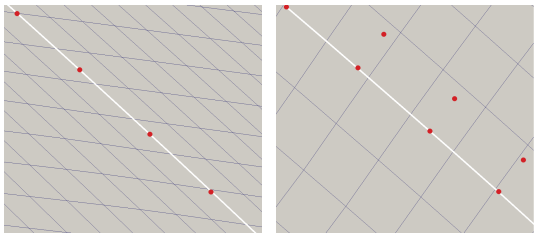

(a) Single row. (b) Double row.

Figure 1: Resulting deformed meshes for a single row and two rows of control points.

there normals opposite to each other. The control points are directly related to the wing shape. Since the wing has a 'zero-thickness' a single row of points can describe the movement of the wing. However as can be seen in Figure 1a, which displays the mesh close to the wing (white line) and the used control points (red dots), using just a single row of control points does not provide the best results in terms of mesh quality as the cells become skewed. Only the translation of each point is captured by the RBF mesh interpolation when using a single row of control points. By introducing a second row of control points close to the wing and perpendicular to the local wing shape, the rotation of the wing is interpolated to the rest of the mesh. This ensures that the cells close to the wing stay perpendicular to the wing, while the rotation is smoothly reduced when moving further away from the wing. This can be seen in Figure 1b. Figure 2 shows the mesh skewness and non-orthogonality for one full f apping period for both a single row of control points and two rows of control points.

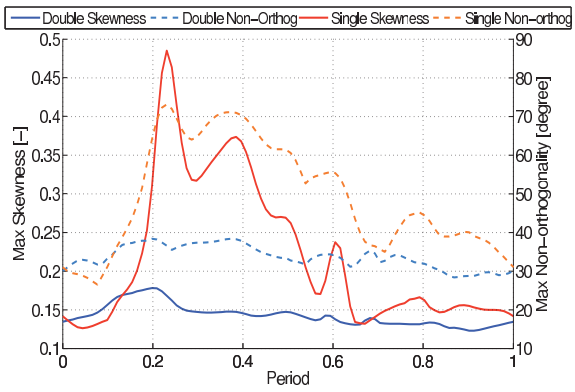

Figure 2: Mesh quality characteristics for single and double row of points.

Non-orthogonality is measured by the angle between the cell centres line (between two cell centres) and the normal of the intermediate face. The degree of skewness is measured as the distance between the face centre and the cross point between the face tangent and the cell centres line. This distance is then normalised with the magnitude of the cell centres line. A schematic explanation can be found in [9]. In OpenFOAM meshes are considered of bad quality when the non-orthogonality is larger than 70 degrees or skewness exceeds 4.0. Considering these two criteria it can clearly be seen that two rows of control points are needed to ensure a good mesh quality during the complete f apping motion. Therefore in all simulations two rows of control points are used. It is clear that RBF mesh interpolation can provide a robust mesh deformation while preserving the original mesh quality.

3 Wing shapes

The wing shapes are extracted from experiments at specif c points in time during a full f apping period. Splines are used to construct the wing shapes in space from the PIV images for specif c points in time. Fourier series are used to interpolate the shape in time.

3.1 The PIV results

From the PIV experiments the chord wise shape at different span-wise locations of the DelFly II wing is obtained [8]. The f apping frequency is 11 Hz, which is characteristic for the DelFly II. At 71% of the span (with a chord of 7.4 cm) 50 shapes in time have been recorded for one full period. Spline interpolation is used to interpolate the wing shape in space for each specif c point in time. In Figure 3 the resulting splines, representing the wing shapes, are shown for the out-stroke or 'peel' phase.

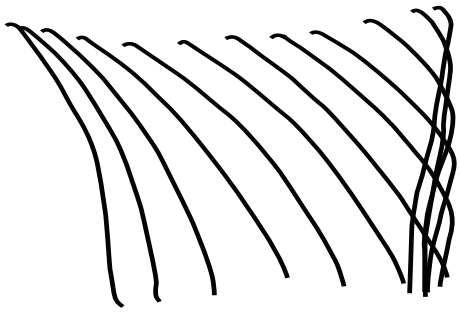

Figure 3: Deforming wing shape for out-stroke obtained from experiments.

3.2 Interpolation in space

For RBF mesh interpolation discrete points in space are needed to function as control points. These discrete points are obtained from the spline interpolations in space. From the continuous description using splines any number of discrete points can be chosen along the wing. Sixty uniformly distributed points along the wing are used as control points for the RBF mesh interpolation. Next step is to interpolate these points in time.

3.3 Interpolation in time

A requirement for the interpolation in time is that the acceleration (second derivative of the interpolation in time) is continuous. If this requirement is not met numerical oscillations will occur in the simulation due to the temporal term in

the Navier-Stokes equation. The temporal term is indirectly related to the pressure gradient. Due to the high accelerations at the wing a high pressure gradient will be present at the wing causing an immediate increase in pressure and thus in the forces. For the interpolation in time Fourier series are used, which ensures that the second derivative is continuous and that the function is periodic. For each coordinate from each control point a Fourier series interpolation is performed in time. In total 120 Fourier series interpolation in time are needed for the 60 points in space. However how many Fourier modes must be taken to interpolate in time? Increasing the number of modes will increase the accuracy of the interpolation through the measured data points, but as the measured data points contain scatter from measurements errors, it will also increase the dominating frequency in the acceleration. High frequencies in the acceleration induce non-physical oscillations into the simulation, which should be prevented at all times.

3.4 Influence of shape interpolation

To determine how many modes must be used both the position error and the inf uence of the acceleration frequency is studied. In Figure 4 the position error with respect to the control points obtained from the experiments is shown for the interpolation in time by means of the maximum normalized maximum error and the maximum normalized 2-norm error. For the normalisation the stroke amplitude is used, which is equal to 8 cm. The 2-norm error is also normalised by the number of points.

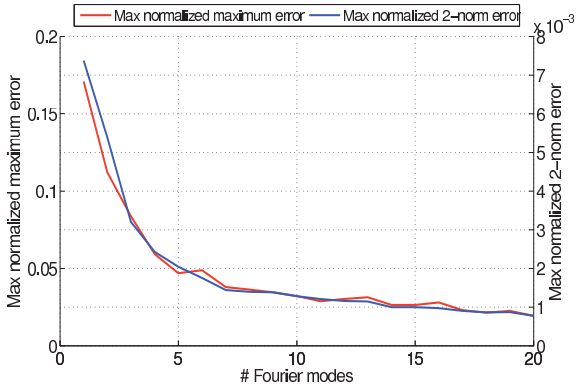

Figure 4: Maximum normalised maximum interpolation error vs. # Fourier modes.

It is clear that both the errors decrease when the number of Fourier modes is increased. When more than 7 modes are used the errors seems to level off and thus using 7 modes for interpolation can be considered suff cient in terms of position error. However using higher modes has a signif cant inf uence on the acceleration of the wing.
In Figure 5 the acceleration in the x-direction of the leading edge is shown for 4, 7 and 10 Fourier modes together with the acceleration of the control point obtained by f nite differencing. The dominating frequency in the acceleration is equal to the highest mode used in the Fourier interpolation. In Figure 6 the periodic average of the upward force for 4, 7 and 10 Fourier modes can be seen. This periodic average is obtained by averaging the force over period 6 till 44.

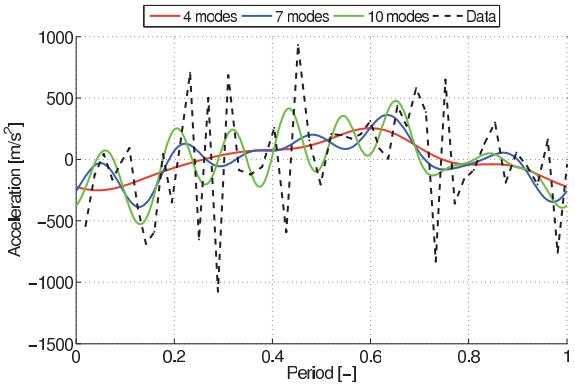

Figure 5: Leading edge acceleration for different number of Fourier modes.

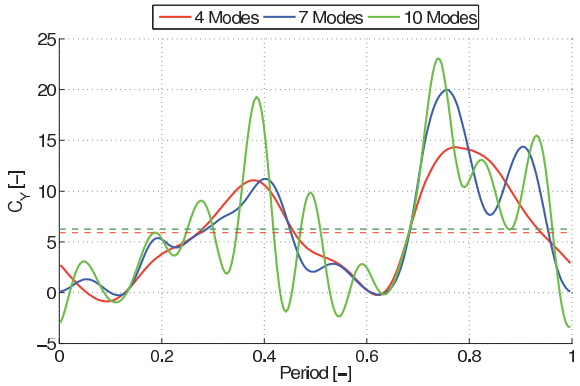

Figure 6: Upward force for different number of Fourier modes.

The dominating frequency in the upward force is equal to the dominating frequency in the acceleration of the wing, which is determined by the highest Fourier mode. Earlier studies (e.g [2]) showed that vortex development and shedding and not the frequency of the wing's acceleration is dominating the force variation. Using the higher Fourier modes for interpolation introduces non-physical oscillations in the pressure f eld and consequently in the forces. To prevent this a DelFly II like wing is simulated by using 4 Fourier modes. This still ensures that general shape of the f exible wing is captured, while the introduction of high frequency oscillations is limited. Further investigation into the selection of the number of Fourier modes is done at a later stage by carefully determining which oscillations are caused by the acceleration and which by the vortex behaviour.

4 Flexible vs. rigid

The influence of the wing flexibility is studied comparing results of the flexible wing with an equivalent rigid wing. Both the upward force and the vortex development and shedding is compared.

4.1 Equivalent rigid wing

To determine the influence of the deforming shape an equivalent rigid wing is needed. No DelFly II experiments were conducted with rigid wings. Therefore an equivalent rigid wing is constructed based on the leading edge and trailing edge movement of the flexible wing. The leading edge motion of the rigid wing is equal to that of the flexible wing. Drawing a line from the leading edge to the trailing edge of the flexible wing gives the direction which is used as pitch angle. With these two parameters (leading edge location and pitching angle in time) and the constant wing length (7.4 cm) the equivalent rigid wing can be modelled during the complete flapping period. In Figure 7 both the flexible and the equivalent rigid wing are shown for different moments in time during the out-stroke.

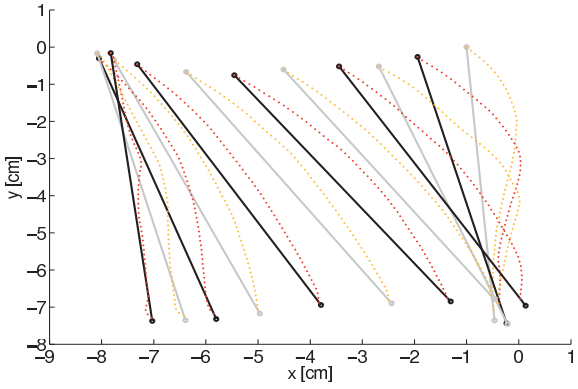

Figure 7: Flexible and equivalent rigid wing.

4.2 Results

For the rigid and flexible wing the forces are calculated for several periods. In total 44 periods are simulated for each calculation. A periodic average is calculated from periods 8 till 44. In Figure 8 the periodic average of the upward force is shown for the three wings. The dashed line is the average force of the period.

Comparing the two wings it can be seen that the average force is higher for the flexible wing. For a large part this is caused by the dip in force for the rigid wing at the start of the out-stroke (around 22% of the flapping cycle). In Figure 9 the vorticity field of the flexible wing is shown at 22% of the period. When this is compared to Figure 10, which is the vorticity field for the rigid wing at the same time, a clear difference is found.

For the flexible wing the leading edge vortex is being formed and the trailing edge vortex is relatively small, causing a positive upward force. A different situation is found for the rigid pitching wing. Here the first leading edge vortex is already shed due to the interaction with the leading edge vortex of the in-stroke, while the trailing edge vortex is still attached and already larger than the one of the flexible wing. Due to this difference the flexible wing produces a significant amount of lift, while the rigid wing has a dip in the upward force. At a later stage (around 40% of the period) the flexible wing start to lose lift due to the developed trailing edge vortex and shedding of the leading edge vortex. Here the rigid wing performs better due to the shedding of the trailing edge vortex and the development of a 'new' leading edge vortex. Here the complex behaviour of interacting vortices leads to the difference in forces. The shape of the wing does have a significant influence on how the vortices develop during the flapping cycle.

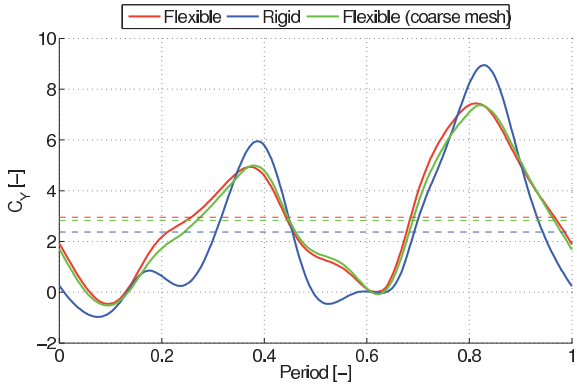

Figure 8: Periodical average of the upward force for the three wings.

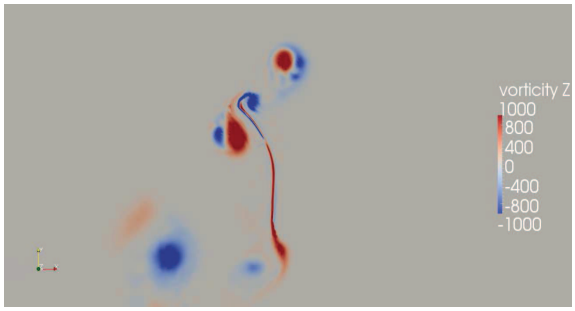

Figure 9: Vorticity field for flexible wing at 22% of the period.

5 'Clap-and-peel' motion

How the 'clap-and-peel' motion influences the upward force production and the vortex development and shedding, is studied by comparing the results of two wings clapping and peeling together with the results obtained in the previous paragraph using a single wing. The wing shapes of the DelFly obtained from the experiments are recorded during the 'clap-

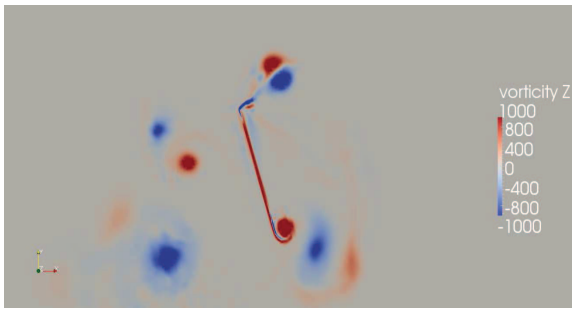

Figure 10: Vorticity field for the rigid wing at 22% of the period.

and-peel' motion and can thus be used in this simulation. In Figure 11 the 'clap-and-peel' motion is illustrated by means of the wing shapes obtained from the experiments.

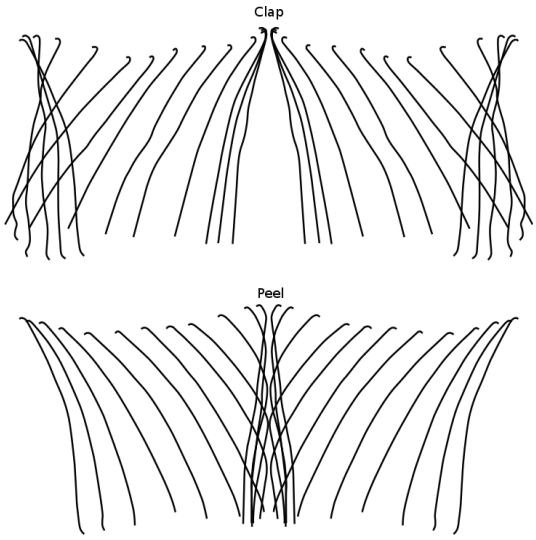

Figure 11: 'Clap-and-peel' motion.

By adding a 'second' wing making the mirrored motion the 'clap-and-peel' is created as can be seen in Figure 11. This can again be done for both the rigid wing and the flexible wing. However the ALE Navier-Stokes method presented earlier has difficulties when two bodies are moving towards each other. Especially when they almost touch each other the cells become very small, which is undesirable. Due to this the mesh quality cannot be preserved any more. Because the 'clap-and-peel' motion of the two wings is symmetric, a symmetry plane together with a single wing performing this motion models the 'clap-and-peel' motion. To impose the symmetry conditions on the correct location an immersed symmetry plane (based on the immersed boundary method) together with mesh topology adjustments near this symmetry plane is used.

5.1 Immersed symmetry plane

Several approaches are available to implement the immersed boundary method [19, 20]. The basis (cell identification) for this method used for this study is developed by Zeljko Tukovic, University of Zagreb, Croatia. A method based on the cut-cell finite volume approach as explained in [20] is implemented. The immersed symmetry plane cuts through a certain set of cells. By changing the shape of these cells an actual finite volume boundary is created in the mesh. In this way the boundary conditions, which are zero gradient for the pressure and slip for the velocity, are enforced at the correct location. Also the boundary conditions are implemented implicitly in the equations in the same way as a for a normal mesh boundary. Each time step this procedure is repeated, because the mesh moves through the immersed symmetry plane. This method is chosen because the mesh quality is not compromised in most of the mesh because the ALE approach with RBF mesh interpolation can still be used. Only the symmetry boundary cells are temporarily changed in shape, which might lead to non-orthogonal cells. In the preliminary results a gap of 3.5% of the chord is used between the wing and the symmetry plane, but the gap can be as small as a single mesh cell. Preliminary results are generated using this method. Further development and validation of this method will be done at a later stage.

5.2 Preliminary results

For both the rigid and the flexible wing results are obtained in terms of the periodic upward force averaged over 38 periods and the vorticity fields. For these simulations only the coarse mesh is used to reduce the computational time, since parallel computing is not yet available. The maximum difference between the two meshes in the periodic averaged upward force for a single wing is 5%. Therefore the coarse mesh can be used for these simulations.
In Figure 12 the periodic average upward force is shown for four cases: the flexible single wing, 'double' flexible wing, rigid single wing and the 'double' rigid wing. The forces shown here are per wing and the dashed line is the integrated force during the single average cycle.

From these results it can be seen that there is a significant difference between the single wing and double wing results. For both the rigid and flexible wing using the 'clap-and-peel' motion increases the upward force produced per wing. Moreover the difference between the rigid and the flexible wing increases when the 'clap-and-peel' motion is applied. For the rigid wing the increase compared to the single wing is approximately 30%, while for the flexible wing it is close to 40%. 'Clap-and-peel' with the flexible wings results in 30% more lift per wing compared to the rigid 'clap-and-fling'. As seen in the single wing cases the development of the leading edge vortices and trailing edge vortices during the out-stroke are of vital importance for the difference in force production. At 30% of the period (in the middle of the out-stroke) the

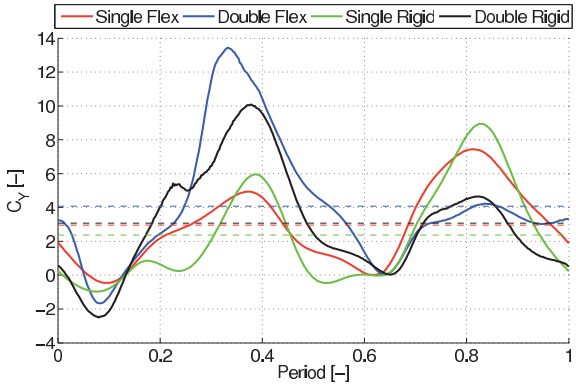

Figure 12: Periodic average upward force for four cases.

difference between the rigid and f exible wing can clearly be seen in case of the 'clap-and-peel' motion. In Figure 13 the vorticity plot of the f exible wing is shown, while in Figure 14 the vorticity of the rigid wing is displayed.

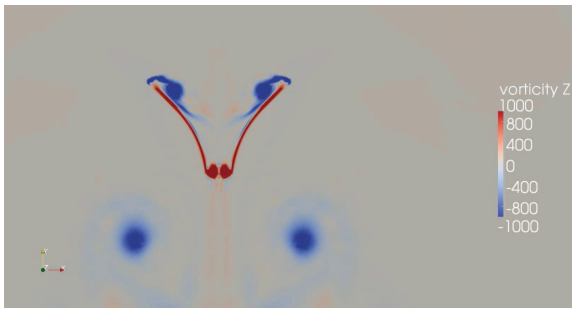

Figure 13: Vorticity f eld for the f exible wing at 30% of the period with immersed symmetry plane.

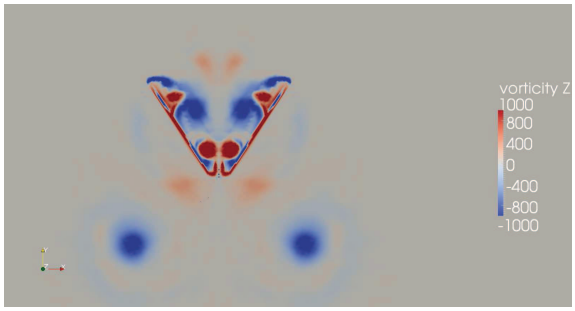

Figure 14: Vorticity f eld for the rigid wing at 30% of the period with immersed symmetry plane.

These plots show that for the rigid wing the leading edge vortex is already shed at this stage, while for the f exible wing this large leading edge vortex is still attached. At a later time in the period the trailing edge vortex will be shed earlier for the f exible wing compared to the rigid wing. These two phenomena explain the higher upward force for the f exible wing. When compared to the single wing vorticity plots (even though they are at different times in the f apping cycle) the main difference is the size and the strength of the leading edge vortex. Due to the strong suction over the leading edge during the 'peel' movement a larger leading edge vortex is created when performing the 'clap-and-peel' motion.

6 Conclusions and Future Work

In this paper the inf uence of wing f exibility and the 'clap-and-peel' motion on the upward force in hover is studied. A single wing, both rigid and f exible, has been simulated using the ALE approach with RBF mesh deformation. The clap-and-peel motion is simulated using an immersed symmetry plane together with the ALE approach for both the f exible and rigid wing. From the preliminary results the following conclusions can be drawn.

- The method of ALE Navier-Stokes together with RBF mesh interpolation provide good mesh quality during the complete f apping cycle when two rows of control points are used.
- Interpolation of the DelFly II wing shapes inf uences the frequency of the resulting forces. This is caused by the acceleration of the wing which is dominated by the highest frequency.
- Both the single wing simulations and the 'clap-and-peel' simulations show an increased upward force for the f exible wing compared to the rigid wing. This is mainly caused by early vortex shedding of the leading edge vortex during the out-stroke for the rigid wing.
- For both the f exible and rigid wing the 'clap-and-peel' motion increases the upward force per wing signif cantly due to the increased size and strength of the leading edge vortex during the out-stroke.

Even though several preliminary conclusions can already be drawn from these results, further studies are needed. The following topics are considered for future analysis.

- Validation of the immersed symmetry plane method by comparing to other methods.
- Simulating different equivalent rigid wings to compare to the f exible wing. It is well known that the pitch angle is important in f apping wings.

Due to the absence of f uid-structure interaction no damping is present in the movement and deformation of the wing. Two-dimensional simulations are known for the earlier shedding of vortices compared to three-dimensional simulations. Therefore a complete three-dimensional f uid-structure simulation together with an experimental study would create an even better insight in the physics. However this study showed which methods can be used for the simulation of the 'clap-and-peel' motion and gives a good insight into the physics of 'clap-and-peel' with f exible and rigid wings.

Acknowledgements

Dr. Zeljko Tukovic, University of Zagreb, Croatia for providing a immersed symmetry plane code for OpenFOAM. Hrvoje Jasak for providing help in setting up OpenFOAM and suggesting OpenFOAM settings.

References

[1] S. Heatcote and I. Gursul. Flexible f apping airfoil propulsion at low reynolds numbers. *AIAA Journal*, 45:1066–1079, 2007.

[2] C.P. Ellington, C. van den Berg, A.P. Willmott, and A.L.R. Thomas. Leading-edge vortices in insect f ight. *Nature*, 384:626–630, 1996.

[3] S. Heathcote and I. Gursul. Flexible f apping airfoil propulsion at low reynolds numbers. *AIAA Journal*, 45:1066–1079, 2007.

[4] H. Aono, S.K. Chimakurthi, P. Wu, E. Sllstrm, B.K. Stanford, C.E.S. Cesnik, P. Ifju, L. Ukeiley, and W. Shyy. A computational and experimental study of f exible f apping wing aerodynamics. In *48th AIAA Aerospace Sciences Meeting*, Orlando, Florida, January 2010. AIAA 2010-554.

[5] Hikaruo Aono, Chang kwon Kang, Carlos E.S. Cesnik, and Wei Shyy. A numerical framework for isotropic and anisotropic f exible f apping wing aerodynamics and aeroelasticity. In *28th AIAA Applied Aerodynamics Conference*, Chicago, Illinois, July 2010. AIAA 2010-5082.

[6] G.C.H.E. de Croon, K.M.E. de Clercq, R. Ruijsink, B. Remes, and C. de Wagter. Design, aerodynamics and vision-based control of the delf y. *International Journal of Micro Air Vehicles*, 1:71–97, 2009.

[7] K.M.E. de Clercq, R. de Kat, B.W. van Remes, B. Oudheusden, and H. Bijl. Flow visualization and force measurements on a hovering f apping-wing mav 'delf y ii'. In *39th AIAA Fluid Dynamics Conference*, San Antonio, Texas, June 2009. AIAA 2009-4035.

[8] M. Groen, B. Bruggeman, B. Remes, R. Ruijsink, B. van Oudheusden, and H. Bijl. Improving f ight performance of the f apping wing mav delf y ii, 2010. International Micro Air Vehicle conference and competitions.

[9] F. Bos. *Numerical simulations of flapping foil and wing aerodynamics*. PhD thesis, Technical University Delft, 2010.

[10] L. Miller and C.S. Peskin. A computational f uid dynamics of 'clap and f ing' in the smallest insects. *The Journal of Experimental Biology*, 208:195–212, 2005.

[11] L.A. Miller and C.S. Peskin. Flexible clap and f ing in tiny insect f ight. *The journal of experimental biology*, 212:3076–3090, 2009.

[12] H. Jasak. *Error analysis and estimation in the finite volume method with applications to fluid flow*. PhD thesis, Imperial College, 1996.

[13] de A. Boer, van der M.S. Schoot, and H. Bijl. Mesh deformation based on radial basis function interpolation. *Computers and Structures*, 85:784–795, 2007.

[14] C.P. Ellington. The novel aerodynamics of insect f ight: applications to micro-air-vehicles. *The Journal of Experimental Biology*, 202:3439–3448, 1999.

[15] W. Shyy, H. Aono, S.K. Chimakurthi, Trizila P., C.-K. Kang, C.E.S. Cesnik, and H. Liu. Recent progress in f apping wing aerodynamics and aeroelasticity. *Progress in Aerospace Sciences*, In Press:1–44, 2010.

[16] J Donea, S. Giuliani, and J.P. Halleux. An arbitrary lagrangian-eulerian f nite element method for transient dynamic f uid-structure interactions. *Computer methods in applied mechanics and engineering*, 33:689–723, 1982.

[17] H. Jasak and Z. Tukovic. Automatic mesh motion for the unstructured f nite volume method. *Transactions of FAMENA*, 30:1–30, 2007.

[18] R. van Loon, P.D. Anderson, F.N. van de Vosse, and S.J. Sherwin. Comparison of various f uid-structure interaction methods for deformable bodies. *Computer and Structures*, 85:833–843, 2007.

[19] H Bandringa. Immersed boundary methods. Master's thesis, University of Groningen, 9700 AK, Groningen, August 2010.

[20] R. Mittal and G. Iaccarino. Immersed boundary methods. *Annual Review of Fluid Mechanics*, 37:239–261, 2005.